Two- and Three-Electron Pauli Spin Blockade in Series-Coupled Triple Quantum Dots

S. Amaha,[1,2,*] W. Izumida,[3] T. Hatano,[2,4] S. Teraoka,[2,5] S. Tarucha,[1,2,5] J. A. Gupta,[6] and D. G. Austing[6]

[1]*RIKEN Advanced Science Institute, RIKEN, 2-1 Hirosawa, Wako, Saitama 351-0198, Japan*

[2]*Quantum Spin Information Project, Japan Science and Technology Agency, ICORP, 3-1, Morinosato, Wakamiya, Atsugi, Kanagawa 243-0198, Japan*

[3]*Department of Physics, Tohoku University, Sendai 980-8578, Japan*

[4]*Nuclear Spin Electronics Project, Japan Science and Technology Agency, ERATO, Sendai 980-8578, Japan*

[5]*Department of Applied Physics, School of Engineering, University of Tokyo, 7-3-1, Hongo, Bunkyo-ku, Tokyo 113-8656, Japan*

[6]*National Research Council of Canada, M50, Montreal Road, Ottawa, Ontario, Canada K1A 0R6*

(Received 31 May 2012; published 2 January 2013)

We investigate two- and three-electron spin blockade in three vertical quantum dots (QDs) coupled in series. Two-electron spin blockade is found in a region where sequential tunneling through all QDs is forbidden but tunneling involving virtual hopping through an empty QD is allowed. It is observed only for the hole cycle with a distinct bias threshold for access to the triplet state. Three-electron spin blockade involving the quadruplet state is observed for nonequibilium conditions where sequential tunneling is allowed *and* the triplet state is accessible. Our results shine light on the importance of the nonequibilium conditions to obtain sufficient population of triplet and quadruplet states necessary for spin blockade.

DOI: 10.1103/PhysRevLett.110.016803 PACS numbers: 73.63.Kv, 73.23.Hk

The spin properties of series-coupled double quantum dots (DQDs) [1,2] have been widely reported. Current suppression by Pauli spin blockade (PSB) [3] in DQDs has proved invaluable for spin manipulation toward quantum computing [1] and for revealing electron spin-nuclear spin coupling [1,4]. Concerning more complex QD systems, spin-related phenomena [5,6] and spin manipulation schemes [7,8] in triple QDs (TQDs) are now attracting much attention. However, current suppression involving quadruplet spin states of three electrons (total spin $S = 3/2$) in series-coupled TQDs with one electron on each QD, quadruplet spin blockade (QSB), has not been reported. There are also as yet few practical guidelines regarding the necessary conditions for achieving fully spin-polarized blockaded states attractive for investigation of spin-related phenomena and spin initialization schemes in TQDs and longer QD chains.

In this Letter, we report on two different spin-blockade mechanisms observed in a few-electron series-coupled vertical TQD device. We first explain the origin of the ''nested'' Coulomb diamond structure and assign charge configurations for a series-coupled TQD and an effective DQD (EDQD) with lowest order sequential tunneling (LO SQT) *via a virtual state*. Two-electron PSB leading to the suppression of the LO SQT in the EDQD is found, and its distinctive appearance is attributable to the population of the triplet state above a bias threshold. QSB is observed in a region where sequential tunneling through the TQD is permitted and the two-electron triplet is accessible in the charge transfer cycle and becomes clear when leakage from the quadruplet state is suppressed in the presence of an external magnetic field. Our results demonstrate the importance of rates governing access to and leakage from spin-blockaded states not only for two-electron PSB [9,10] but also for three-electron QSB and spin blockade in longer QD chains.

Figure 1(a) shows a schematic of the TQD device. The three QDs are embedded in a submicron circular mesa, made from a $GaAs/Al_{0.22}Ga_{0.78}As/In_{0.05}Ga_{0.95}As$ quadruple-barrier triple-quantum-well resonant tunnel structure sandwiched by n-doped GaAs source and drain contacts, and surrounded by a single Schottky gate. The outer (inner) barriers are 8.0 nm (4.0 nm) thick, and the outer wells (center well) are (is) 12.5 nm (14.5 nm) thick. Based on a self-consistent calculation for zero bias, the lowest energy center-well level is anticipated to be $\sim$1.3 meV above the lowest energy outer-well levels, and the tunnel coupling between adjacent wells (QDs) is estimated to be $\sim$0.5 meV [11]. We measure the dc current I as a function of source-drain voltage V_{sd} and gate voltage V_g at a temperature $<$100 mK with a magnetic (B) field applied perpendicular to the current. Figures 1(b) and 1(c), respectively, show the observed current I and the differential conductance dI/dV_{sd} as a function of (V_{sd}, V_g) at $B = 0$ T. In Fig. 1(b), irregular-shaped and apparently open Coulomb diamonds are observed near pinch-off (total number of electrons, $N = 0$). However, in Fig. 1(c), closed Coulomb diamonds can be seen near pinch-off.

To reproduce the asymmetric Coulomb diamond pattern, the dot energy levels need to be suitably arranged at $V_{sd} = 0$ V [with ''staircase'' configuration—see Fig. 1(a)—as determined below]. Similar to vertical DQDs [3], the misaligned dot energy levels are likely attributable to device processing and random impurity potential in the material [11]. To quantify the energy level arrangement and to identify charge states, we extend the constant interaction (CI) model for DQDs [3] to TQDs [11] to calculate

 © 2013 American Physical Society

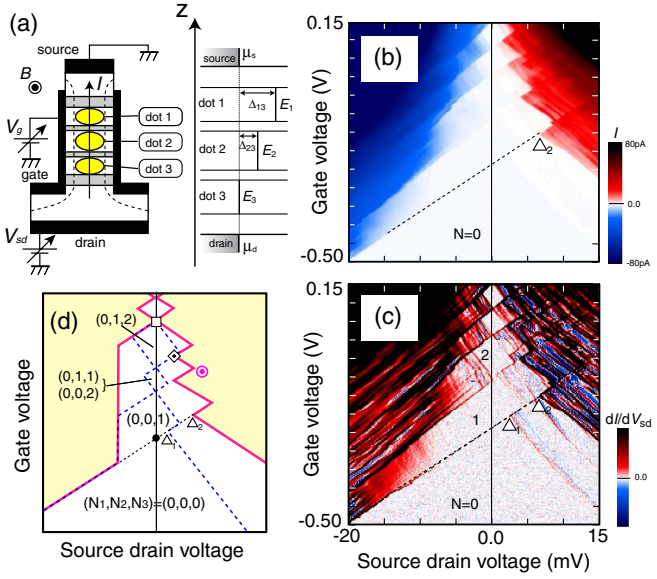

FIG. 1 (color online). (a) (Left) Schematic of TQD. Electrons in the QDs are confined in the vertical direction by heterostructure barriers and in the lateral direction by an approximate two-dimensional harmonic potential. (Right) Schematic of empty dot levels E_1, E_2, and E_3 at point filled circle identified in (d). Δ_{13} (Δ_{23}) is the offset energy between E_1 and E_3 (E_2 and E_3) and at point filled circle $\Delta_{13} = U = 2\delta$ and $\Delta_{23} = V = \delta$. (b) Measured I and (c) dI/dV_{sd} as a function of (V_{sd}, V_g) at $B = 0$ T. (d) Coulomb diamond pattern calculated with CI model. Yellow areas with pink border lines denote regions where sequential tunneling through all three QDs is possible [leading to strong current features clear in (b)]. Dashed blue lines identify Coulomb diamonds for EDQD [clear in (c)] requiring LO SQT through dot 1. Features Δ_1 and Δ_2 characteristic of EDQD and TQD, respectively, in (c) are also well reproduced and reflect the finite value of Δ_{23} and Δ_{13}, respectively.

Coulomb diamond patterns. The intradot Coulomb interaction in each dot, U, and the interdot Coulomb interaction between dot i and dot j, V_{ij} ($i, j = 1, 2, 3, i \neq j$) are constants. We set $V_{12} = V_{23} = V_{13} = V = U/2$ for simplicity [3,11], where typically $U \sim 5$ meV in vertical QDs. We assume the energy of the QD levels varies linearly with V_{sd} and the gate equally affects each dot. We observe weak ($I < 1$ pA) features near $V_{sd} \sim 0$ V and $N \leq 3$ nested between strong ($I > 10$ pA) features [Figs. 1(b) and 1(c)], so here dot 1 is always empty (energy level of dot 1 is inaccessible from source or drain). However, if higher order virtual tunneling processes between the source and dot 2 via dot 1 are permitted, weak nested features are expected for tunneling through EDQD consisting of source-dot 2-dot 3-drain. The virtual tunneling process can be represented by an effective tunneling barrier between the source and dot 2 in EDQD, which is significantly thicker than the tunnel barrier between dot 3 and the drain. By application of CI model for EDQD, we reproduce the shape of the observed nested Coulomb diamonds for sequential tunneling through EDQD [dashed blue lines in Fig. 1(d) below feature open square], and determine the lowest energy level in dot 2 (E_2) is offset above the lowest energy level in dot 3 (E_3) at $V_{sd} = 0$ V by energy $\Delta_{23} = E_2 - E_3 \sim V(= \delta)$. Next, by application of the CI model for TQD, we reproduce the threshold for sequential tunneling in a TQD [pink lines in Fig. 1(d)], and determine the lowest energy level in dot 1 (E_1) is offset above E_3 at $V_{sd} = 0$ V by energy $\Delta_{13} = E_1 - E_3 \sim U(= 2\delta)$. The calculated TQD and EDQD Coulomb diamonds are shown together in Fig. 1(d). We can now assign charge configurations (N_1, N_2, N_3) ($N = N_1 + N_2 + N_3$) for the Coulomb blockaded regions, where N_1, N_2, and N_3, respectively, are the number of electrons in dot 1, dot 2, and dot 3. To recap: the closed Coulomb diamonds nested inside the open Coulomb diamonds in Figs. 1(b) and 1(c) are attributed to EDQD [3,12]. Sequential tunneling through all three dots is expected only in the yellow areas in Fig. 1(d).

However, some details of the observed Coulomb diamonds cannot be reproduced with the CI models. Most notable is the distinctive quadrilateral-shaped region of current suppression ($I \sim 0.2$ pA), which is seen near the $N = 2$ Coulomb diamond magnified in Fig. 2(a). This region, outlined in red and labeled with filled diamond, is attached to the upper-right side of the $N = 2$ Coulomb diamond. For forward bias, the electron cycle near α is $(0, 0, 1) \rightarrow (0, 1, 1) \rightarrow (0, 0, 2) \rightarrow (0, 0, 1)$, and the hole

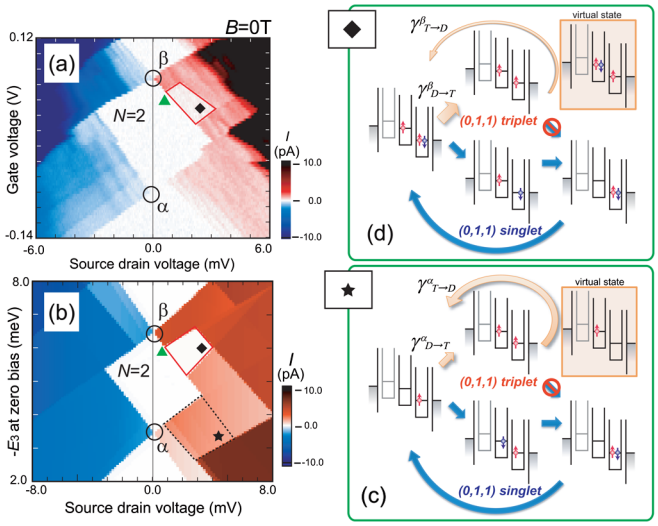

FIG. 2 (color online). (a) Magnified plot of measured I near $N = 2$ Coulomb diamond at $B = 0$ T. (b) Calculated current through TQD by master equation approach based on EDQD model reproducing key features in (a). Parameters are $U = 4$ meV, $V_{23} = 2$ meV, $t_{23} = 0.4$ meV, $\Gamma_d = 0.2$ μeV, $\Gamma_s^{\text{eff}}/\Gamma_d \sim 4 \times 10^{-2}$, $T = 100$ mK (T is electron temperature). The relaxation rate between same-spin states is taken to be a constant $\gamma \sim 0.6$ meV. At zero bias $\Delta_{23} = E_2 - E_3 = 2$ meV, and E_3 at zero bias is given relative to the chemical potential of the source and drain at equilibrium. The region labeled filled diamond observed in (a) is well reproduced in (b). (c) [(d)] Schematic of relevant charge and spin states in the region labeled filled star [filled diamond] identified in (b) for charge transfer cycle in forward bias near α [β].

cycle near β is (0, 1, 2) → (0, 1, 1) → (0, 0, 2) → (0, 1, 2). We stress that direct tunneling to dot 1 plays no role in the nested Coulomb diamond structure. As for the charge transfer process (1, 1) → (0, 2) in a DQD, the charge transfer process (0, 1, 1) → (0, 0, 2) in a TQD is expected to be forbidden by Pauli exclusion if the spin state is a triplet [3]. However, the appearance of the current suppression is clearly different from the typically encountered chevron-shaped region in vertical DQDs [3]. Two notable features of the observed current suppression region are the following: (i) it is seen only for the hole cycle but not for the electron cycle [13], and (ii) there is a distinct V_{sd} threshold (labeled with a green filled upward triangle).

To understand features (i) and (ii), we calculate the current through EDQD with a master equation formalism taking discrete dot levels and spin into account [14,15]. For the TQD, we assume one single-particle level in each dot for simplicity and define the tunnel coupling between dot 1 and dot 2 (dot 2 and dot 3) to be $t_{12}(t_{23})$, and the strength of the coupling between the source and dot 1 (drain and dot 3) to be $\Gamma_s(\Gamma_d)$. In our TQD device [11], based on nominal parameters for the structure, we estimate $t_{12} = t_{23} \sim 0.5$ meV, and $\Gamma_s \sim \Gamma_d$. For EDQD, we introduce an effective coupling strength between the source and dot 2, $\Gamma_s^{\rm eff}$, which corresponds to the energy width of the LO SQT process via dot 1. Using a second-order perturbation approximation for this process, $\Gamma_s^{\rm eff}$ is evaluated to be $(\frac{t_{12}}{\Delta_{13}-\Delta_{23}})^2\Gamma_s \sim (\frac{t_{12}}{\delta})^2\Gamma_d$ [14]. Accordingly $\Gamma_s^{\rm eff}/\Gamma_d$ is estimated to be $\sim 10^{-2}$–10^{-1} [16]. Figure 2(b) presents a numerical calculation of the current for $\Gamma_s^{\rm eff}/\Gamma_d = 4 \times 10^{-2}$ [17] and reproduces features (i) and (ii) experimentally observed [18].

Regarding the orgin of (i), we examine transition rates to enter into and escape from the (0,1,1) triplet for charge transfer cycles near α and β. Figures 2(c) and 2(d) shows a schematic of the relevant charge and spin states for charge transfer cycles near α [β]. Note that in the following discussion of the transition rates at 0 T, we have neglected the spin degeneracy factors for compactness but included them in the numerical calculations. Near α, specifically in the region labeled filled star [see Fig. 2(b)], access to the (0,1,1) triplet is from the (0,0,1) doublet, with transition rate $\gamma^{\alpha}_{D\to T} \sim \frac{\Gamma_s^{\rm eff}}{\hbar}$. The return process is via the virtual (0,1,0)-doublet state, and the rate is $\gamma^{\alpha}_{T\to D} \sim (\frac{t_{23}}{\Delta_{23}})^2 \frac{\Gamma_d}{\hbar}$. Since for our TQD $\Gamma_s^{\rm eff} \sim (\frac{t_{12}}{\delta})^2\Gamma_d$, $t_{12} = t_{23}$ [19], and $\Delta_{23} = \delta$, $\gamma^{\alpha}_{T\to D}$ is expected to be comparable to $\gamma^{\alpha}_{D\to T}$ [$\gamma^{\alpha}_{T\to D}/\gamma^{\alpha}_{D\to T} \sim 1$]. Consequently the triplet state population cannot build up sufficiently for strong current suppression by PSB to occur near α. Near β, specifically in the region labeled filled diamond, access to the (0,1,1) triplet is from the (0,1,2) doublet, with transition rate $\gamma^{\beta}_{D\to T} \sim \frac{\Gamma_d}{\hbar}$ ($> \gamma^{\alpha}_{D\to T}$). The return process is via the virtual (0,2,1)-doublet state, and the rate is $\gamma^{\beta}_{T\to D} \sim (\frac{t_{23}}{\Delta_{23}})^2 \frac{\Gamma_s^{\rm eff}}{\hbar}$ ($< \gamma^{\alpha}_{T\to D}$). Crucially $\gamma^{\beta}_{T\to D}$ is much smaller than $\gamma^{\beta}_{D\to T}$ [$\gamma^{\beta}_{T\to D}/\gamma^{\beta}_{D\to T} \sim \eta^2$, where $\eta \cong (t_{12}/\delta)^2$]. Consequently the triplet state population can build up strongly, and so strong current suppression by PSB is expected only near β [16].

Turning to the origin of (ii), Fig. 3(a) shows an I-V_{sd} cross section through the region labeled filled diamond at 0 T. Coulomb blockade is lifted at low V_{sd} [region (1): pink], but at higher V_{sd}, current is suppressed [region (2): blue]. The current stripe in region (1), just above the Coulomb blockade, and the distinct V_{sd} threshold for the current suppression, linked to the boundary line labeled with the green filled upward triangle in Fig. 3(b), have not been previously encountered for PSB in DQDs [3]. Because the interdot coupling in our EDQD ($t_{23} \sim 0.5$ meV) is stronger than that in typical DQDs (< 0.15 meV [1,3,4]) exhibiting PSB, (0,1,1)-singlet and (0,0,2)-singlet states are more strongly hybridized to form bonding and antibonding singlet states. Hence, near zero bias, the bonding singlet is expected to be located energetically below the (0,1,1) triplet by $\Delta E_{\rm ST} = \sqrt{2}t_{23} \sim 0.7$ meV. Consequently, because of strong stabilization of the bonding singlet, only the bonding-singlet state is accessible from the (0,1,2) doublet in the charge transfer cycle at low V_{sd} near β, and so the current can flow via the bonding singlet without the strong population of the (0,1,1) triplet. However, when the chemical potential in the drain is lowered sufficiently ($V_{sd}/4 > \Delta E_{\rm ST}$), the (0,1,1) triplet additionally becomes accessible and the charge transfer cycle will be interupted by PSB [20], leading to current suppression in region (2). In our device, $\Delta E_{\rm ST}$ is sufficiently large that only the (0,1,1) bonding singlet is accessible at low bias, and so there is a clear threshold at higher bias to access the (0,1,1) triplet. The observed B-field

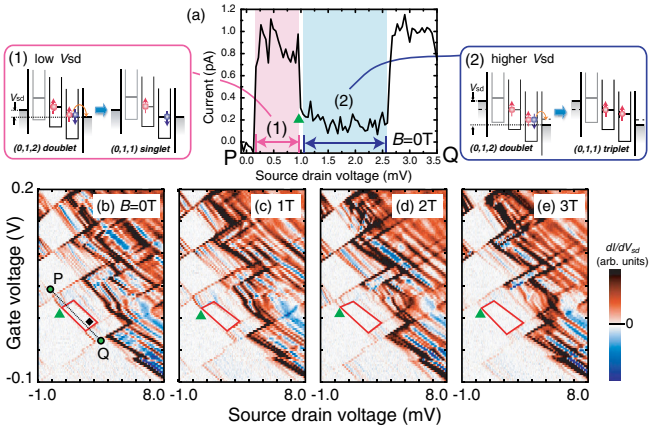

FIG. 3 (color online). (a) I-V_{sd} cross section through the region labeled filled diamond of suppressed current near β for $B = 0$ T. Position of cross section P-Q is identified in (b). Schematics of transfer process (1) through the (0,1,1) bonding singlet energetically allowed at low bias and of transfer process (2) through (0,1,1) triplet energetically allowed *only* at higher bias (to right of boundary line filled upward triangle) are also shown. (b)–(e) dI/dV_{sd} as a function of (V_{sd}, V_g) for $B = 0$ T–3 T. Boundary filled upward triangle of region filled diamond shifts toward zero bias as B field is increased.

dependence of the boundary line labeled with the green filled upward triangle in Figs. 3(b), 3(d), and 3(e) also confirms our picture. By applying a B field perpendicular to the current, t_{23} can be reduced by diamagnetic localization leading to a reduction of ΔE_{ST} [21]. Consequently the boundary line labeled with the green filled upward triangle slides along the upper-right side of the $N = 2$ Coulomb diamond toward zero bias as the B field is increased.

Next we describe the QSB mechanism in the TQD [13]. Our asymmetric TQD with staircase configuration [Fig. 1(a)] provides easy access to states with double occupancy of dots required to see QSB. To the high bias side of the line between ◈ and pink ◉ in Fig. 1(d), sequential tunneling through all three QDs is allowed, and charge transfer involving cycle (A) $(0, 1, 2) \rightarrow (0, 1, 1) \rightarrow (1, 1, 1) \rightarrow (0, 2, 1) \rightarrow (0, 1, 2)$ and cycle (B) $(0, 1, 2) \rightarrow (0, 1, 1) \rightarrow (0, 0, 2) \rightarrow (1, 0, 2) \rightarrow (0, 1, 2)$ are expected from the TQD CI model. To the high bias side of the boundary line labeled with the green filled upward triangle [also identified in Figs. 2(a) and 2(b)], the (0,1,1) triplet becomes accessible for the transfer process $(0, 1, 2) \rightarrow (0, 1, 1)$ common to both (A) and (B). Crucially, $(0, 1, 1) \rightarrow (0, 0, 2)$ is not allowed for the triplet state by PSB, so (B) is no longer active when the (0,1,1) triplet is accessed, and this allows us to focus on (A) in the following discussion. Note that if the (1,1,1) quadruplet state becomes populated, the transfer process $(1, 1, 1) \rightarrow (0, 2, 1)$ in (A) is not allowed by Pauli exclusion resulting in current suppression. Figure 4(a) shows a schematic of the charge and spin states relevant to QSB accessible in (A). The region where the three-electron high spin state (1,1,1) quadruplet is accessible via the (0,1,1) triplet leading to current suppression is labeled with open diamond

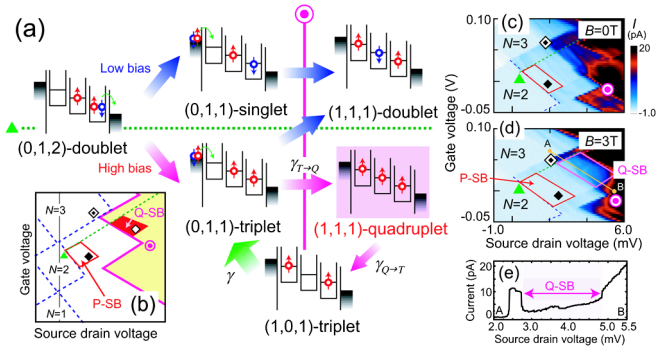

FIG. 4 (color online). (a) Schematic of charge and spin states relevant to observed three-electron QSB. (b) Coulomb diamond pattern from CI models with added regions marked, respectively, filled diamond and open diamond where two-electron PSB in the LO SQT regime and three-electron QSB in the sequential tunneling regime should occur. To the high bias side of boundary line green filled upward triangle *and* boundary line between ◈ and pink ◉, the (1,1,1) quadruplet is accessible via the (0,1,1) triplet. The most significant step to release QSB is from the (1,1,1) quadruplet to the (1,0,1) triplet. Magnified plot of measured I in the region where three-electron QSB is expected at $B = 0$ T (c) and 3 T (d). (e) I-V_{sd} cross section A-B identified in (d) at $B = 3$ T.

in Fig. 4(b) [16]. However, the observed current is only slightly suppressed at $B = 0$ T as shown in Fig. 4(c). Following the approach applied to two-electron PSB in EDQD, we evaluate the transition rates between (1,1,1) quadruplet and relevant triplet states. Access to the (1,1,1) quadruplet is principally from the (0,1,1) triplet, and the transition rate is $\gamma_{T\rightarrow Q} \sim \frac{\Gamma_s}{\hbar}$. The most significant step to release QSB is from the (1,1,1) quadruplet to the (1,0,1) triplet and the transition rate is $\gamma_{Q\rightarrow T} \sim (\frac{t_{23}}{\delta})^2 \frac{\Gamma_d}{\hbar}$ [6,16]. The (1,0,1) does not contribute to the charge transfer cycle according to the TQD CI model but is quantum mechanically accessible and energetically allowed as a two-electron delocalized triplet excited state [16]. The return to the (0,1,1) triplet from the (1,0,1) triplet involves rapid relaxation by phonon emission at a rate γ expected to greatly exceed $\gamma_{Q\rightarrow T}$, and therefore the net transition rate to return from the (1,1,1) quadruplet to the (0,1,1) triplet is set by $\gamma_{Q\rightarrow T}$ [16]. $\gamma_{Q\rightarrow T}$ is clearly smaller than $\gamma_{T\rightarrow Q}$, but the ratio $\gamma_{Q\rightarrow T}/\gamma_{T\rightarrow Q} \sim \eta$ is larger (smaller) than $\gamma^{\beta}_{T\rightarrow D}/\gamma^{\beta}_{D\rightarrow T} \sim \eta^2$ ($\gamma^{\alpha}_{T\rightarrow D}/\gamma^{\alpha}_{D\rightarrow T} \sim 1$) relevant to the discussion of two-electron PSB in the LO SQT regime; i.e., the QSB region may not be as clear as the PSB region [22]. However, applying a B field, η is expected to become smaller owing to the diamagnetic localization effect, resulting in a reduction of leakage from the blockaded (1,1,1) quadruplet and increased visibility of the QSB region [21]. Compared to 0 T [Fig. 4(c)], 3 T [Fig. 4(d)] is found to be sufficient to reveal the QSB region clearly [see also Fig. 4(e)]. This result further demonstrates the importance of the ratio of transition rates for access and return processes to observe QSB clearly and of the contribution of delocalized molecular states in TQDs [16,23].

Finally, we comment on spin blockade in longer QD chains by extending our findings on the TQD. The release process from the spin-blockaded state with one electron on each QD, $(1, \ldots, 1, 1, 1)$, is dominated by that to $(1, \ldots, 1, 0, 1)$ involving quantum mechanical tunneling via virtual states and its rate, evaluated in the same way as for the DQD and TQD, is $\gamma_{\text{release}} \sim (\frac{t}{\delta})^2 \frac{\Gamma_d}{\hbar}$ [16]. For observable sequential tunneling current, stronger interdot tunnel coupling is required as the number of QDs is increased, and this results in a stronger release of spin blockade. LO SQT is therefore a significant contributing factor limiting the observation of spin blockade. Our results highlight the importance of engineering access and leakage rates by adjusting the energy level configuration and tunnel couplings to achieve robust spin blockade in QD chains.

In conclusion, we investigated spin-blockade properties of an asymmetric series-coupled TQD. Characteristic features of the two-electron PSB observed in EDQD were explained in terms of transition rates for access to and leakage from the spin-blockaded (0,1,1)-triplet involving LO SQT processes. In the region where sequential tunneling through the TQD is allowed *and* the (0,1,1) triplet is accessible, current suppression by QSB was observed.

The suppression was enhanced by reducing leakage from the (1,1,1) quadruplet to molecular TQD triplet states with a perpendicular B field. Our results are important for engineering access and leakage rates to achieve robust spin blockade advantageous for spin-related phenomena and spin initialization in DQDs, TQDs, and longer QD chains.

We thank G. C. Aers, Y. Nishikawa, A. Oguri, K. Ono, K. Kono, T. Kubo, and Y. Tokura for discussions. Part of this work is supported by the Grant-in-Aid for Young Scientists B (No. 23740248 and No. 22740191) from the Japan Society for the Promotion of Science (JSPS), a Grant-in-Aid for Scientific Research S (No. 19104007) from JSPS, a Grant-in-Aid for Scientific Research on Innovative Areas (21102003) from Ministry of Education Culture, Sports, Science and Technology, Japan, Funding Program for World-Leading Innovative R&D on Science and Technology (FIRST), ERATO-JST (080300000477), and IARPA project ''Multi-Qubit Coherent Operations'' through Copenhagen University.

*Corresponding author.
s-amaha@riken.jp

[1] R. Hanson, L. P. Kouwenhoven, J. R. Petta, S. Tarucha, and L. M. K. Vandersypen, Rev. Mod. Phys. **79**, 1217 (2007).
[2] W. G. van der Wiel, S. D. Franceschi, J. M. Elzerman, T. Fujisawa, S. Tarucha, and L. P. Kouwenhoven, Rev. Mod. Phys. **75**, 1 (2002).
[3] K. Ono, D. G. Austing, Y. Tokura, and S. Tarucha, Science **297**, 1313 (2002).
[4] K. Ono and S. Tarucha, Phys. Rev. Lett. **92**, 256803 (2004).
[5] Some recent representative examples are the following: D. S. Saraga and D. Loss, Phys. Rev. Lett. **90**, 166803 (2003); J. Kim, D. V. Melnikov, J. P. Leburton, D. G. Austing, and S. Tarucha, Phys. Rev. B **74**, 035307 (2006); M. Korkusinski, I. P. Gimenez, P. Hawrylak, L. Gaudreau, S. A. Studenikin, and A. S. Sachrajda, Phys. Rev. B **75**, 115301 (2007); K. L. Hur, P. Recher, E. Dupont, and D. Loss, Phys. Rev. Lett. **96**, 106803 (2006); Y.-P. Shim and P. Hawrylak, Phys. Rev. B **78**, 165317 (2008); M. Busl, R. Sanchez, and G. Platero, Phys. Rev. B **81**, 121306(R) (2010); A. Oguri, S. Amaha, Y. Nishikawa, T. Numata, M. Shimamoto, A. C. Hewson, and S. Tarucha, Phys. Rev. B **83**, 205304 (2011).
[6] C.-Y. Hsieh, Y.-P. Shim, and P. Hawrylak, Phys. Rev. B **85**, 085309 (2012).
[7] E. A. Laird, J. M. Taylor, D. P. DiVincenzo, C. M. Marcus, M. P. Hanson, and A. C. Gossard, Phys. Rev. B **82**, 075403 (2010); L. Gaudreau, G. Granger, A. Kam, G. C. Aers, S. A. Studenikin, P. Zawadzki, M. Pioro-Ladrière, Z. R. Wasilewski, and A. S. Sachrajda, Nat. Phys. **8**, 54 (2012).
[8] D. Schröer, A. D. Greentree, L. Gaudreau, K. Eberl, L. C. L. Hollenberg, J. P. Kotthaus, and S. Ludwig, Phys. Rev. B **76**, 075306 (2007); G. Granger, L. Gaudreau, A. Kam, M. Pioro-Ladrière, S. A. Studenikin, Z. R. Wasilewski, P. Zawadzki, and A. S. Sachrajda, Phys. Rev. B **82**, 075304 (2010); S. Amaha, T. Hatano, H. Tamura, S. Teraoka, T. Kubo, Y. Tokura, D. G. Austing, and S. Tarucha, Phys. Rev. B **85**, 081301(R) (2012).
[9] J. Iñarrea, G. Platero, and A. H. MacDonald, Phys. Rev. B **76**, 085329 (2007); B. Muralidharan and S. Datta, Phys. Rev. B **76**, 035432 (2007); A. B. Vorontsov and M. G. Vavilov, Phys. Rev. Lett. **101**, 226805 (2008).
[10] F. Qassemi, W. A. Coish, and F. K. Wilhelm, Phys. Rev. Lett. **102**, 176806 (2009).
[11] S. Amaha, T. Hatano, W. Izumida, S. Teraoka, K. Ono, K. Kono, S. Tarucha, G. C. Aers, J. A. Gupta, and D. G. Austing, Jpn. J. Appl. Phys. **51**, 02BJ06 (2012).
[12] T. Ota, K. Ono, M. Stopa, T. Hatano, S. Tarucha, H. Z. Song, Y. Nakata, T. Miyazawa, T. Ohshima, and N. Yokoyama, Phys. Rev. Lett. **93**, 066801 (2004); A. Fuhrer, L. E. Fröberg, J. N. Pedersen, M. W. Larsson, A. Wacker, M. -E. Pistol, and L. Samuelson, Nano Lett. **7**, 243 (2007); S. Amaha, T. Kodera, T. Hatano, K. Ono, Y. Tokura, S. Tarucha, J. A. Gupta, and D. G. Austing, J. Phys. Soc. Jpn. **80**, 023701 (2011).
[13] In Fig. 2(a), the current just to the right of α is observed to be much weaker than the current just to the right of β. This is reproduced in Fig. 2(b) and is discussed in the Supplemental Material at http://link.aps.org/supplemental/10.1103/PhysRevLett.110.016803.
[14] V. N. Golovach and D. Loss, Phys. Rev. B **69**, 245327 (2004).
[15] J. Fransson and M. Råsander, Phys. Rev. B **73**, 205333 (2006).
[16] See Supplemental Material at http://link.aps.org/supplemental/10.1103/PhysRevLett.110.016803 for additional discussion and calculations.
[17] In a realistic system spin relaxation processes involving hyperfine coupling and spin-orbit interactions will also influence the current; however, in our calculations, these relaxation processes are not taken in account.
[18] The four boundaries of the region labeled filled diamond are formally defined in the Supplemental Material at http://link.aps.org/supplemental/10.1103/PhysRevLett.110.016803.
[19] To be definite in the analysis of the transition rates, we assume $t_{12} = t_{23}$; however, this is not a critical assumption. The asymmetry in the current suppression regions near α and β is primarily driven by the ratio $\Gamma_s^{\mathrm{eff}}/\Gamma_d$, which is determined by the factor $(\frac{t_{12}}{\delta})^2$ in our model (see also Fig. S1 in the Supplemental Material at http://link.aps.org/supplemental/10.1103/PhysRevLett.110.016803).
[20] M. R. Buitelaar, J. Fransson, A. L. Cantone, C. G. Smith, D. Anderson, G. A. C. Jones, A. Ardavan, A. N. Khlobystov, A. A. R. Watt, K. Porfyrakis, and G. A. D. Briggs, Phys. Rev. B **77**, 245439 (2008).
[21] We assign the perpendicular B-field dependence in Figs. 3(b)–3(d), 3(c), 3(e), 4(c), and 4(d) to diamagnetic localization and have neglected any influence of Zeeman splitting.
[22] Realistically, as discussed in Ref. [6], the presence of excited states in dot 3 can enhance the leakage current, but the influence of these states is also suppressed with B field owing to the reduction of effective tunneling by diagmagnetic localization.
[23] For a more detailed understanding, processes including the release of spin blockade through the hyperfine interaction and more than one single-particle level per QD would have to be included [S. Amaha *et al.* (unpublished)].